Power System Technology **Volume 46 · Number 2 · 2022**
ISSN: 1000-3673

PLL Parameter Optimization Design for Renewable Energy Grid-connected Inverters in Weak Grid

Yan P., Ge X., Wang H., Sun W., Zhu Y.
1. Department of Mechanical Engineering, King Saud University P.O. Box 800, Riyadh 11421, Saudi Arabia
2. Universite de Lille, UML Unite Mecanique de Lille Villeneuve d'Ascq, France

ABSTRACT
In order to construct a 3D rotor model, periodicity and Multiple Reference Frame (MRF) strategies were applied to address full Computational Fluid Dynamics (CFD) that incorporate the Reynolds-averaged Navier–Stokes (RANS) equations. A simulation model was run to examine the power of the wind turbines, both including and excluding the hub and tower. The purpose of this was to identify an approach that would decrease the computational time cost of wind turbine simulation. Firstly, a full-scale horizontal axis wind turbine simulation was carried out, and subsequently, comparisons were made with the results of the wind tunnel experiment utilizing the K-omega SST and Sparlat Allmaras viscosity models. The results were compared to determine the optimum model with the lowest simulation time and highest accuracy to the experimental results. Following this, the complete models' simulation was compared to the model excluding the hub and tower in order to check the disparity in the results of the two. Additionally, to ascertain the computational cost saving, the ratio of the two simulation times was established. The findings show that the two models produce results that correspond well to the experimental results, and that the power coefficient had a greater value for the complete model than the simple model. Furthermore, it was found that the power coefficient values of the full model have significantly higher levels of similarity to the experimental values. The Sparlat Allmaras and K-omega SST viscosity models returned error percentages of 0.52% and 12.6% respectively. For the partial model utilizing the same computer device, a 5.7% error rate was recorded, with a computational time saving of approximately 34%.

1. INTRODUCTION

Due to the growing reliance on renewable sources of energy, there is an increasing importance placed on dependable simulation results for the mass production of wind turbines. Accurately ascertaining the reason for disparities in the results of simulations and experiments is becoming as significant as actually minimizing the difference. In addition to manufacturing, enhancing the efficiency of present wind farms is a leading issue [1-5].

Opportunities to increase the lifespan of current wind farms are arising through focusing on partial repowering rather than entire overhauls. Either way, dependable simulation results are critical components of the design cycle process [6-10]. In simulations such as this, atmospheric aspects become the simulation variables. They include the atmospheric boundary layer, temperature stratification, air density, and effect of convection, all of which are external elements. Design elements also play a key role. These include the impact of the airfoil choice on the efficiency of the wind turbine, the height of the wind turbine, and the effect of the hub. Other elements, including performance and simplicity of production, are also being given more weight [11].

Wind turbine performance is impacted by design factors. Blade design has been an area of focus for researchers. Numerical analysis of wind turbines facilitates acquiring an overview of its operations, with the analytical outcomes providing a start point for analysis. However, a vast array of research results must be obtained, which is both costly and time-consuming. As blade design has evolved and been optimized, designs have been made available by the National Renewable Energy Laboratory (NREL) and the National Advisory Committee for Aeronautics (NACA), which are utilized globally. Nevertheless, in contrast to other renewable sources of energy like solar power, more straightforward but less renowned wind turbine designs are also popular. These simpler designs are highly efficient and enable uncomplicated manufacturing. Consequently, researchers must assess all potential designs rather than having a singular focus.

Another significant aspect is the impact of the wind tower and hub, which this paper comprehensively investigates. The wind turbine performance in relation to power is estimated as the final product is the electrical power that is supplied to a grid station for monitoring as per the energy needs. This necessitates calculating the work done by the wind on a wind turbine (its velocity) and ascertaining the power the wind turbine generates for a particular wind speed. As shown in Figure 1, the wind decelerates when passing through a wind turbine, and this velocity loss is the work done, i.e., the force acting on the blades of the wind turbine when a fixed mass, meaning a fixed air volume, passes through that turbine.

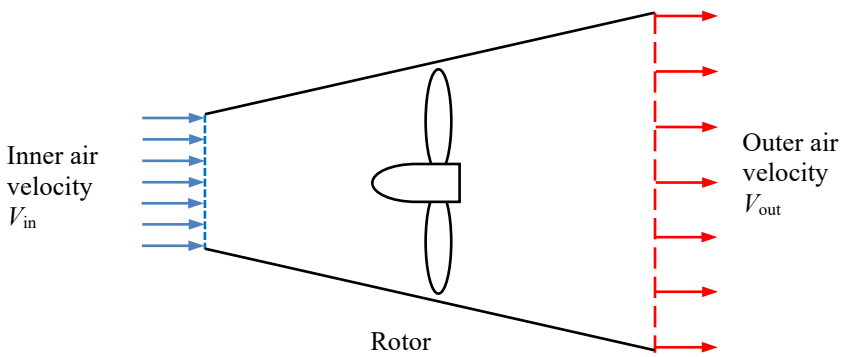

Figure 1: Air velocity change in the wind turbine

A successful formula is one that offers the most straightforward means of acquiring the desired answer. Newton was especially talented in this context; the Second Law of Motion can establish the force, power, and energy needed for a turbine to function. By determining the volume of air displaced, a wind turbines' power can be estimated.

$$E = F \times S \tag{1}$$

where:
E represents the work done to the moving object from rest
S represents the distance
F represents the force

However, as it is impossible to measure during constant operation, it is unrealistic to include the distance travelled by a fixed air mass in the wind turbine formula. Additionally, this distance is not a necessary component due to Newton's Second Law of Motion and the third equation of motion, which allows force and wind speed to be linked directly. The following equation merges equation (1) with force $F = ma$ as per Newton's Second Law:

$$E = m \times a \times s \tag{2}$$

Employing the third equation of motion: $v^2 = 2as$, the following can be obtained:

$$a = \frac{v^2}{2s} \tag{3}$$

where:
a represents the acceleration (m/s^2)

Substituting this into equation (2), the kinetic energy of a mass in motion can be expressed as:

$$E = \frac{1}{2}mv^2 \tag{4}$$

Power is calculated as:

$$P = \frac{dE}{dt} = \frac{1}{2}\frac{dm}{dt}v^2 \tag{5}$$

where:
$\frac{dm}{dt}$ represents the mass flow rate given by $(A.v)$

Hence:

$$P = \frac{1}{2}\rho A v^3 \tag{6}$$

where:
P represents the mechanical power
ρ represents the air density
A represents the area swept by the rotor blades
v represents the air velocity
C_p represents the power coefficient

Power is in proportion to the cube of velocity, air density, and the rotor swept area (πr^2). Therefore, the factors that have the most effect on wind power are the air quantity, the airspeed, the air mass, and the diameter of the rotor [12]. The air quantity refers to the volume that is controllable by the area swept by the blade of the wind turbine. The airspeed is influenced by the placement and configuration of the wind turbine and the choice of location. The air density is impacted by both the location and the environment. The power rises in line with the square of the rotor diameter and the cube of the wind speed, with the latter being more significant. Figure 2 illustrates the rise in the power with the wind speed and the rotor diameter [13].

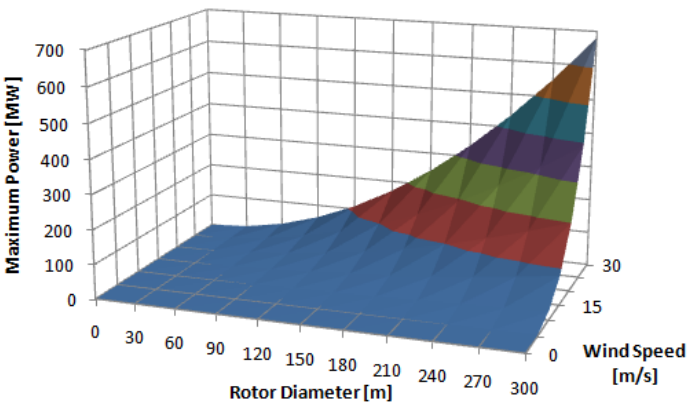

Figure 2: The effect of wind speed and rotor diameter on the maximum power extracted from the wind turbine [13]

It is impossible for the velocity of the wind to be zero when it passes the wind turbine. According to Betz's Law, which was introduced by Albert Betz in 1919, a wind turbine can convert a maximum of 59.26% of the kinetic energy of the wind into mechanical energy. This is applicable to both horizontal and vertical wind turbines [14]. The maximum amount of power that can be extracted from the wind is the highest theoretical value of the coefficient of power. In reality, a wind turbine will have an efficiency level of 35%-45%. Electrical, frictional, and bearing losses cause the losses from the Betz constant. Hence, in optimum conditions, a maximum of 59.26% of the wind's energy can be extracted by the wind turbine. The coefficient of power (C_p) refers to the power extracted by the turbine (Pt) divided by the total power of the wind resource (Pw).

$$C_{p_{max}} = \frac{P_t}{P_W} = \frac{16}{27} \approx 0.5926 \quad (7)$$

In this study, the coefficient of power is utilized as the primary basis for comparisons. The coefficient of power of a specific wind turbine fluctuates according to the particular operating conditions, which include the input wind speed, turbine angular speed, and blade design. It is an indicator of the general level of efficiency of the particular wind turbine and is frequently employed by the wind power industry [15]. The coefficient of power can be expressed as:

$$C_p = \frac{Torque \ * \ Angular \ Velcoity}{0.5AR\rho V_{inlet}^2}$$

Equation (6) provides the turbine power; therefore, incorporating it can be given as:

$$P = \frac{1}{2}\rho A v^3 C_p \quad (8)$$

As illustrated in equation (8), an increase in the velocity v has a massive impact on the power. Accordingly, the majority of developments are tailored towards raising the velocity by increasing the airflow through the swept area. There have been additional advancements to enhance the wind turbines' power output. The initial action was to raise the height of the wind turbine tower in order to reach higher airflow speeds, particularly in urban areas where buildings and other constructions can impede the ease of wind flow and create obstacles that decrease the wind turbines' rotational speed.

The early wind turbines have been analysed using fluid dynamics in an attempt to establish the level of force necessary to displace a mass of air to a particular distance. This differs from mechanical work only in that the work being carried out by the turbine is done through creating lift in moving air. Thus, after passing through the wind turbine, the wind speed will have less energy as some of it is used to rotate the turbine. The earlier discussion shows that more knowledge is required about the way in which the air will be displaced. In a wind turbine, the most significant aspect of blade design is the airfoil selection, as the blades' airfoil must be capable of facilitating high lift with low drag. Accordingly, essential considerations for optimal performance in wind turbine design include an airfoil with a high lift to drag ratio, the blade quantity, and the airfoil angle of attack. The torque generated provides an indicator of the wind turbines' performance. Therefore, an improvement target for wind power machines is harvesting more kinetic energy to raise the total converted power output [6]. Calculating the coefficient of torque can be expressed as:

$$C_q = \frac{Torque}{0.5AR\rho V_{inlet}^2}$$

Contextually, the discussion above is in relation to velocity differential upstream and downstream of the wind turbine.

The relationship between the velocities of the rotor blade and the relative wind is referred to as the tip speed ratio (λ). It is determined by the following three elements: (i) the radius of the blades' swept area; (ii) the rotational velocity of the rotor (ω); (iii) the wind velocity (v_w) [13]. The following equation is the initial design parameter, and forms the basis for the calculation of all other optimal rotor dimensions:

$$\lambda = \frac{\omega.r}{v_w} \tag{9}$$

Some considerations when determining the optimum tip speed ratio are aerodynamics, mechanical stress, torque, noise, and efficiency [6]. There are some important components of the structure of horizontal axis wind turbines that enhance both the efficiency and the amount of power extracted from the wind [16].

Antonini et al. [17] put forward a Computational Fluid Dynamics (CFD) model that utilizes the actuator disk technique to streamline the wind turbines' simulation process and the approximation of the surface boundary layer. This approach was employed in three different wind farms, and comparisons were made between the results and the available experimental measurements' values. It was found that the proposed approach greatly enhanced the computational fluid dynamics predictions with the available experimental measurements. Furthermore, the researchers stated the variance in terms of the results of past studies could be attributable to the uncertainty in the wind direction that was reported in the datasets. In a study based in Horns Rev offshore wind farm, Naderi et al. [18] investigated the modelling of horizontal axis wind turbine wakes. They employed an enhanced actuator disk model in combination with computational fluid dynamics. They calculated the total induction factor and actual upstream velocity for each turbine. The improved model was separate from the thrust coefficient curve. The results showed that the steady-state wake models' precision was substantially improved. Blade Element Momentum (BEM) theory [19] forecasts the local forces exerted on a rotor or wind turbine blade. Additionally, BEM can perform several complex calculations of the resultant velocities at the blades. Various studies advanced the standard BEM theory by augmenting it with the impacts of several elements in order to enhance its precision. Others merged BEM theory with CFD so as to reduce the simulation time. Numerous studies examined diverse wind turbine parameters, such as alternative blade designs [20-23], and the minimum and maximum wake loss and output power production, respectively [24, 25]. Researchers have also attempted to determine how the efficiency is impacted by various internal and external forces [26, 27], and how the overall wind turbine performance is affected by ice, sand, and blade roughness. Other studies have examined the effect of the hub and tower in the context of the wake flow [28-32]. The authors determined that they needed to formulate means of streamlining the calculations of the interaction forces and momentum on the wind turbine components so as to reduce the simulation durations for all lateral studies. However, it remains critical that the results are dependable. Even when utilizing high parallel computing (HPC), wind turbine simulations are very time-consuming. Computational costs rise as the size and complexity of the wind turbine increase.

The goal of this study is to create a simulation model for wind turbines that decreases computational time. The study is performed in the context of the simulation time cost with the power extraction coefficient, and for the first time, endeavours to reduce the components with the lowest impact on the power coefficient. The starting point is the investigation of a

complete 3D model including the hub and tower. The next stage is to examine a partial model of the turbine excluding the hub and tower. Time could be saved in the simulation by reducing the number of components with the lowest effect on the process of harvesting the wind power and developing the wake.

2. GOVERNING EQUATIONS

A CFD utilizes the differential form of the Navier-Stokes equations to address the pressure and velocity via a control volumes' mass and momentum conservation equations. The mass change must be zero, thus the mass derivative can be expressed as:

$$\frac{dM}{dt} = \dot{m}_{in} - \dot{m}_{out} \tag{10}$$

If $\dot{m}_{in} - \dot{m}_{out} = 0$, it means that:

$$\frac{dM}{dt} = 0 \tag{11}$$

Therefore:

$$M = const \tag{12}$$

The mass and momentum equations are applied to develop the continuity equation, which is given as:

Continuity Equation

$$\frac{D\rho}{Dt} + \rho \frac{\partial U_i}{\partial x_i} = 0 \tag{13}$$

Momentum Equation

$$\rho \frac{\partial U_j}{\partial t} + \rho U_i \frac{\partial U_j}{\partial x_i} = -\frac{\partial P}{\partial x_j} - \frac{\partial \tau_{ij}}{\partial x_i} + \rho g_j \tag{14}$$

where:

$\rho \frac{\partial U_j}{\partial t}$ represents the local change with time

$\rho U_i \frac{\partial U_j}{\partial x_i}$ represents the momentum convection

$\frac{\partial P}{\partial x_j}$ represents the surface force

$\frac{\partial \tau_{ij}}{\partial x_i}$ represents the molecular-dependent momentum change, i.e., diffusion

ρg_j represents the mass force

$$\tau_{ij} = -\mu\left(\frac{\partial U_j}{\partial x_i} + \frac{\partial U_i}{\partial x_j}\right) + \frac{2}{3}\delta_{ij}\mu\frac{\partial U_k}{\partial x_k} \tag{15}$$

In the case that the fluid is incompressible, the continuity and momentum equations can be expressed as follows:

Continuity Equation

$$\frac{\partial U_i}{\partial x_i} = 0 \tag{16}$$

Momentum Equation

$$\rho\frac{\partial U_j}{\partial t} + \rho U_i\frac{\partial U_j}{\partial x_i} = -\frac{\partial P}{\partial x_j} - \mu\frac{\partial^2 U_j}{\partial x_i^2} + \rho g_j \tag{17}$$

This simulation uses the K-omega Shear Stress Transport (SST) viscosity. This turbulence model is a two-equation eddy viscosity model that is frequently used in the aerodynamics field. It is also commonly applied for industrial purposes and can be utilized for achieving a low Reynolds number without a damping function. Additionally, the model has proved effective in simulations of airflow around a hairy cylinder, and strong correlations have been identified between numerical results and experimental test data [33]. It is a hybrid model that merges th $k-\omega$ e and the $k-\varepsilon$ models, thereby reaping the benefits of both. The $k-\omega$ and $k-\varepsilon$ models are activated by the F1 blending function near the wall and in the free stream, respectively. Consequently, the $k-\varepsilon$ model is a good fit with the flow simulations in the viscous sub-layer. Simultaneously, the $k-\varepsilon$ model effectively predicts flow behavior away from the wall.

The following governing equations are written as [34]:

Turbulence Kinetic Energy

$$\frac{\partial k}{\partial t} + U_j\frac{\partial k}{\partial x_j} = P_k - \beta^* k\omega + \frac{\partial}{\partial x_j}\left[(\nu + \sigma_k\nu_T)\frac{\partial k}{\partial x_j}\right] \tag{19}$$

Specific Dissipation Rate

$$\frac{\partial \omega}{\partial t} + U_j\frac{\partial \omega}{\partial x_j} = \alpha S^2 - \beta\omega^2 + \frac{\partial}{\partial x_j}\left[(\nu + \sigma_\omega\nu_T)\frac{\partial \omega}{\partial x_j}\right] + 2(1-F_1)\sigma_{\omega 2}\frac{1}{\omega}\frac{\partial k}{\partial x_i}\frac{\partial \omega}{\partial x_i} \tag{20}$$

F_1 (Blending Function)

$$F_1 = \tanh\left\{\left\{\min\left[max\left(\frac{\sqrt{k}}{\beta^*\omega y}, \frac{500\nu}{y^2\omega}\right), \frac{4\sigma_{\omega 2}k}{CD_{k\omega}y^2}\right]\right\}^4\right\} \tag{21}$$

$F_1 = 1$ inside the boundary layer and 0 in the freestream.

CD_{kw}

$$CD_{k\omega} = max\left(2\rho\sigma_{\omega 2}\frac{1}{\omega}\frac{\partial k}{\partial x_i}\frac{\partial \omega}{\partial x_i}, 10^{-10}\right) \quad (22)$$

Kinematic Eddy Viscosity

$$\nu_T = \frac{a_1 k}{max(a_1\omega, SF_2)} \quad (23)$$

F_2 (Second Blending Function)

$$F_2 = tanh\left[\left[max\left(\frac{2\sqrt{k}}{\beta^*\omega y}, \frac{500\nu}{y^2\omega}\right)\right]^2\right] \quad (24)$$

P_K *(Production Limiter)*

$$P_k = min\left(\tau_{ij}\frac{\partial U_i}{\partial x_j}, 10\beta^* k\omega\right) \quad (25)$$

The simulation includes the use of the Sparlat Allmaras viscosity model.

In the Sparlat Allmaras viscosity model $\tilde{\nu}$, the transported variable total is equal to the turbulent kinematic viscosity, except in the vicinity of the near-wall, which is a viscosity-impacted region. The transport equation for $\tilde{\nu}$ is written as:

$$\frac{\partial}{\partial t}(\rho\tilde{\nu}) + \frac{\partial}{\partial x_i}(\rho\tilde{\nu}u_i) = G_\nu + \frac{1}{\sigma_{\tilde{\nu}}}\left[\frac{\partial}{\partial x_j}\left\{(\mu + \rho\tilde{\nu})\frac{\partial\tilde{\nu}}{\partial x_j}\right\} + C_{b2}\rho\left(\frac{\partial\tilde{\nu}}{\partial x_j}\right)^2\right] - Y_\nu + S_{\tilde{\nu}} \quad (26)$$

where:
G_ν represents the production of turbulent viscosity in the near-wall area caused by $\sigma_{\tilde{\nu}}$
Y_ν represents the destruction of turbulent viscosity in the near-wall area caused by $\sigma_{\tilde{\nu}}$
$\sigma_{\tilde{\nu}}$ represents wall blocking and viscous damping
C_{b2} represents a constant
ν represents the molecular kinematic viscosity
$S_{\tilde{\nu}}$ represents a user-defined source term

3. THE WIND TURBINE SIMULATION MODEL

In this study, the rotor under investigation was selected from an open-source wind turbine family created by Hugh Piggott. This model is used globally in many organizations, and in excess of 1,000 turbines have been built (Engineers Without Borders UK, Wind Empowerment). The chief design objectives are durability, cost-efficiency, ease of construction, economic sustainability, effectiveness at low to medium wind speeds (3-10 m/s), and capability of surviving extreme weather [34]. Its ease of construction and efficiency are the key reasons for its prevalence, as it does not require any complex or expensive machinery. The blade geometry was modelled in CATIA®. Ansys Fluent® was used for meshing and analyses. Both transient and steady-state simulations were carried out. Mesh motion facilitated enhanced results, particularly for wake analysis. Figure 3 depicts the geometry of the selected blade model being developed.

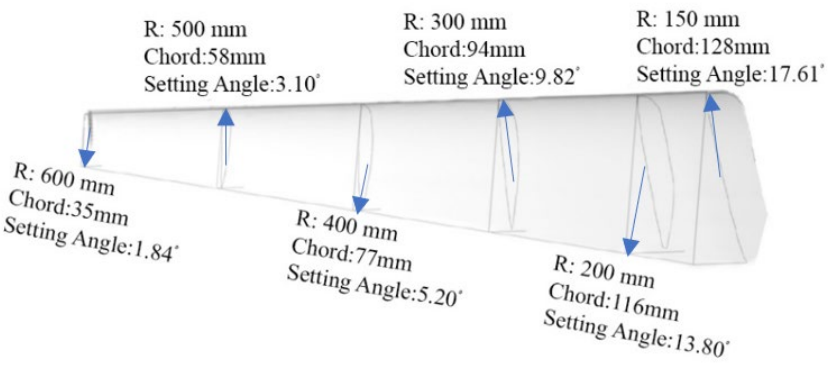

Figure 3: Blade Geometry

3.1 Turbine Model including Tower and Hub

Table 1 presents the parameters applied for the tower and hub. So as to define a rotating vantage point, the complete blades and hub were situated in an enclosure. Figure 4 illustrates the geometry of the blades with the hub, while Figure 5 presents the complete model of the turbine, including the tower and hub.

Table 1: Parameters for the tower and hub

	Part	Dimension (mm)
1	Hub diameter	200
2	Turbine total diameter	1200
3	Tower height	3000

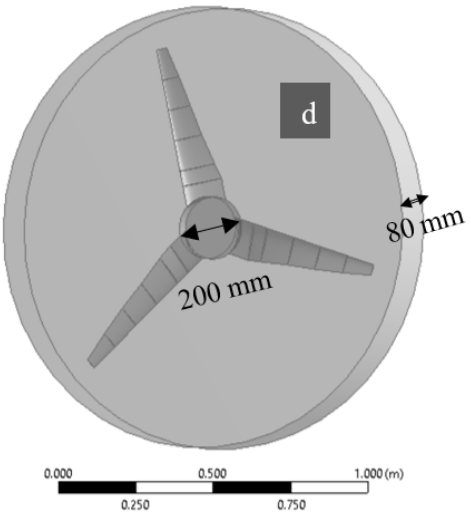

Figure 4: The geometry of the blades with the hub

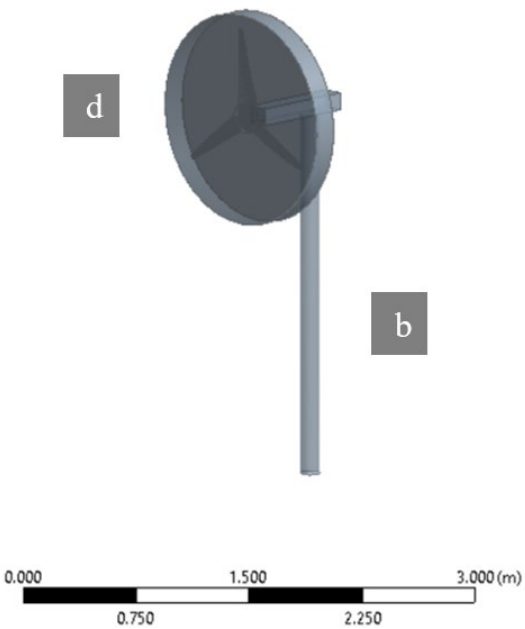

Figure 5: Complete geometry modelling including the tower and hub

Figure 6 shows the computational domain with two zones for the complete turbine model. The external stationary zone and the internal zone show the tunnel and the inner area rotating zone housing the turbine, respectively.

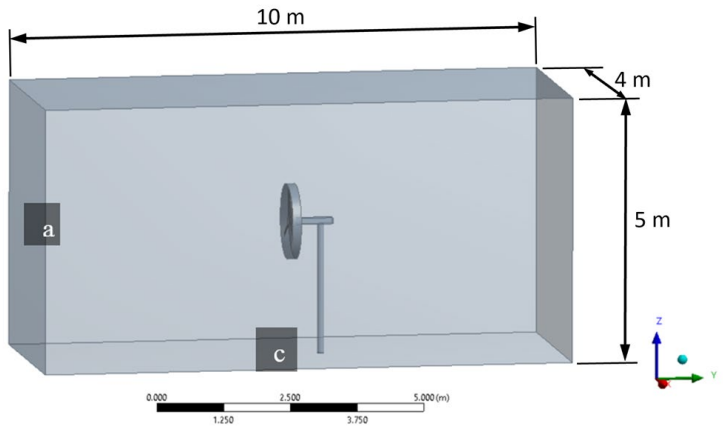

Figure 6: Formulation of domain with two zones

3.2. Turbine Meshing

A CFD was used to carry out the meshing process for the complete turbine model. Mesh motion was employed, which entails complete mesh, inclusive of the turbine, traveling at 0.005 step size. Trihedral is the type of mesh used here as shown in Figure 7. In terms of the mesh sizing, it was thin, close to the blades, and medium in the outer zone.

The selection of domains facilitated straightforward monitoring of the impact of the wake. As depicted in Figures 4 and 6 (above), the rotating domain and stationary domain lengths are 80 mm and 10 m, respectively. The meshing and various zones were labelled the inlet, outlet, turbine, tower, ground, and rotating domains (see Figure 8).

To enable the examination of the mesh sensitivity, four mesh refinements were carried out to establish the mesh dependency on results until the rate of change was minimal. The details of this are presented in both Figure 9 and Table 2.

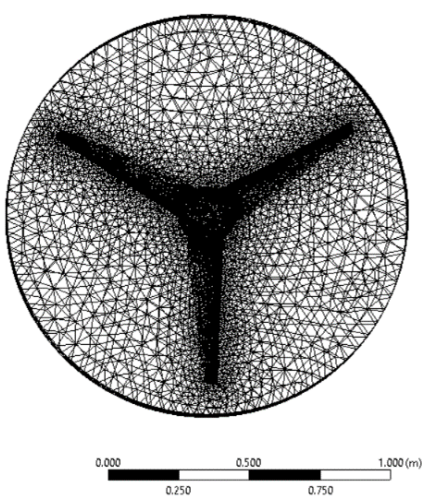

Figure 7: Meshing of the rotating domain

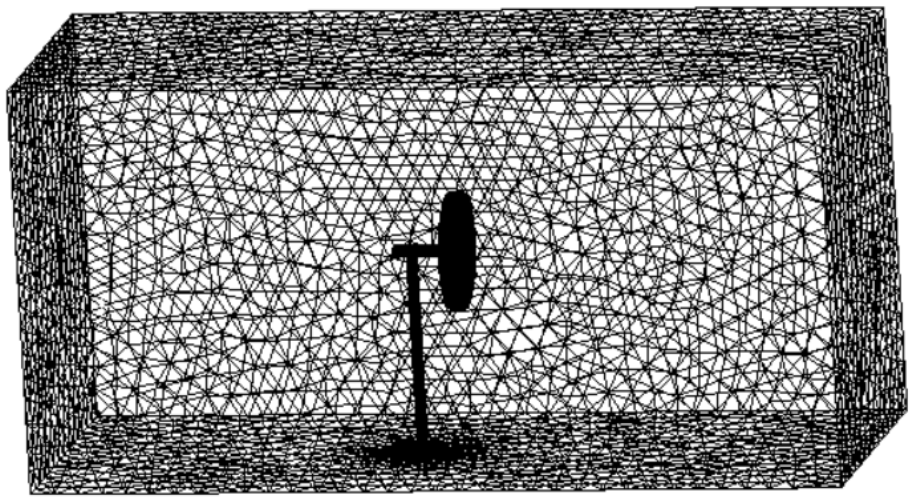

Figure 8: Meshing of the computational domain

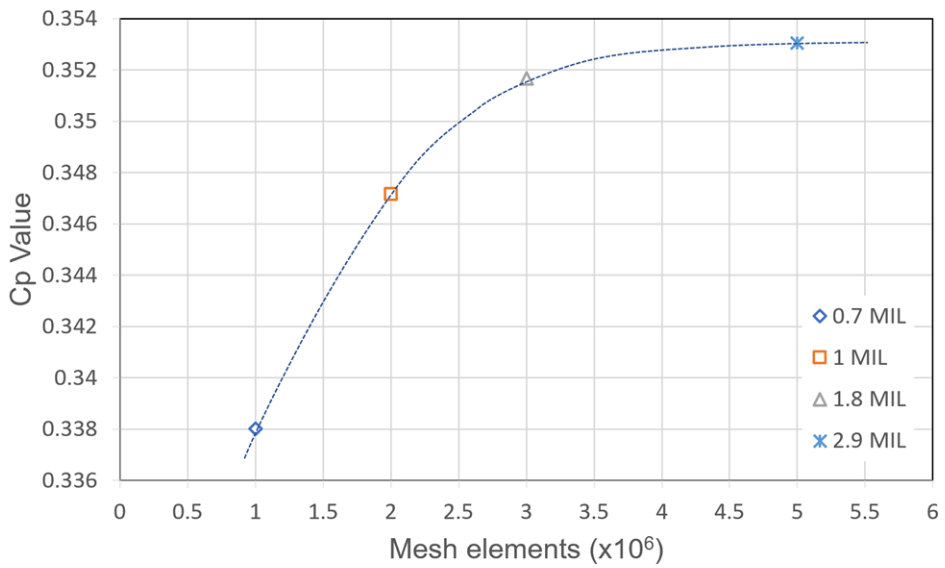

Figure 9: Mesh independence results

Table 2: Mesh independence values

RPM	Inlet Velocity	Mesh Elements (million)	Torque (N.m)	Power (watt)	Cp	Tip Speed Ratio
40	5.5	0.7	0.939	37.568	0.359	4.364
		1.1	0.890	35.580	0.340	4.364
		2	0.832	33.290	0.318	4.364
		2.5	0.828	33.120	0.316	4.364
		3	0.832	33.272	0.318	4.364

3.3. Boundary Conditions

The boundary conditions linked to Figures 4, 5, and 6 above that were applied for the simulation are presented below in Table 3.

Table 3: Boundary conditions

a	Inlet velocity	5.5 m/s
b	Tower	Stationary Wall
c	Ground	Wall
d	Rotating Domain	Different RPM for Different Tip Speed Ratio

The inlet is designated a velocity of 5.5 m/s, while the ground is allocated wall BC. The rotating components are considered interfaces to interact between the stationary and rotating domains. The two rotating domains are assigned a 40-rpm frame motion. The outlet is allocated a pressure outlet. In order to facilitate comparison with the other results, the rotating domain speed was set at 5.5 m/s. The reason for the choice of this level is that it is a moderate wind speed that is approximate to the typical wind speed in the Saudi Arabia.

3.4. Solver Setup

The numerical solver setup in this study was chosen to solve the domain, and the blade employed two forms of viscous models: (i) SST $K-\omega$; (ii) Sparlat Allmaras. The solver will simultaneously solve the continuity and Navier-Stokes equation utilizing the dual approach. As a result, this will reduce the overall total iterations, thereby using less iterations for each simulation. However, this system necessitates more processor power. The u, v, and w velocities were solved using spatial discretization. The least-square cell-based square method was used to calculate the residual of the equations. Discretization schemes include second order and first order. The solver adds a transient term when solving equations via pseudo transient, which enables convergent solutions to be reached more quickly. Furthermore, multigrid errors are rapidly damped out as higher term relaxation is switched on.

4. RESULTS AND MODEL VALIDATION

4.1. Turbine Model Validation

Steady-state analysis has facilitated verification to be conducted. Simulation is iterated until the point that the blade surface monitors show that the movement generated by the turbine has converged entirely. Figures 10 and 11 present the simulation results.

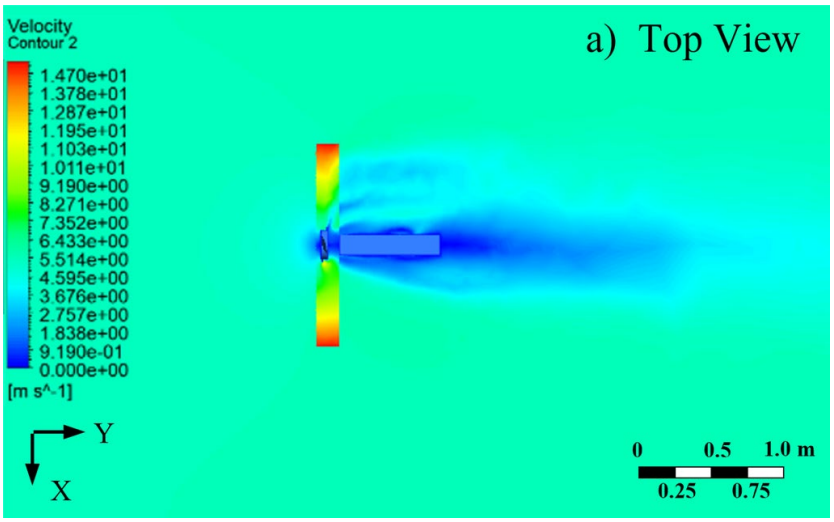

(a) Top view

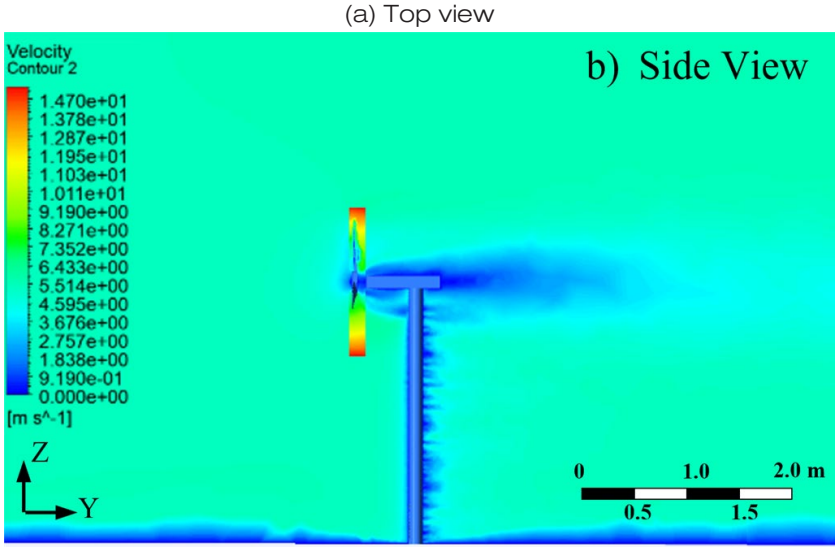

(b) side view

Figures 10: Velocity contours. (a) top view, (b) side view

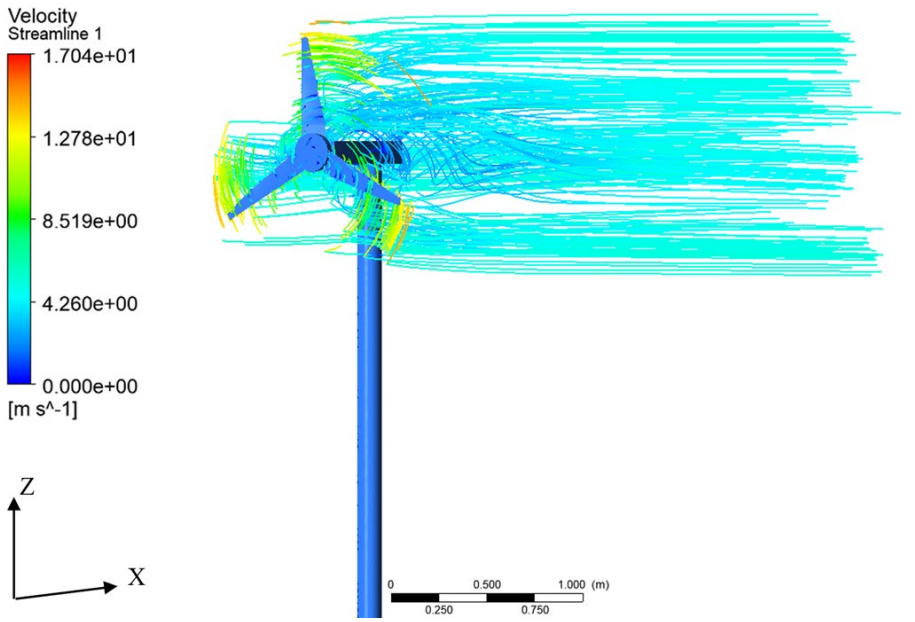

Figure 11: Velocity streamlines

As presented in Figure 12, the Sparlat Allmaras and K-omega SST models enabled viscous model independence. The blue and orange curves represent the K-omega SST and Sparlat Allmaras models, respectively. The Sparlat Allmaras model is highly comparable to the experimental results [35] and is more computationally effective than the K-omega SST model.

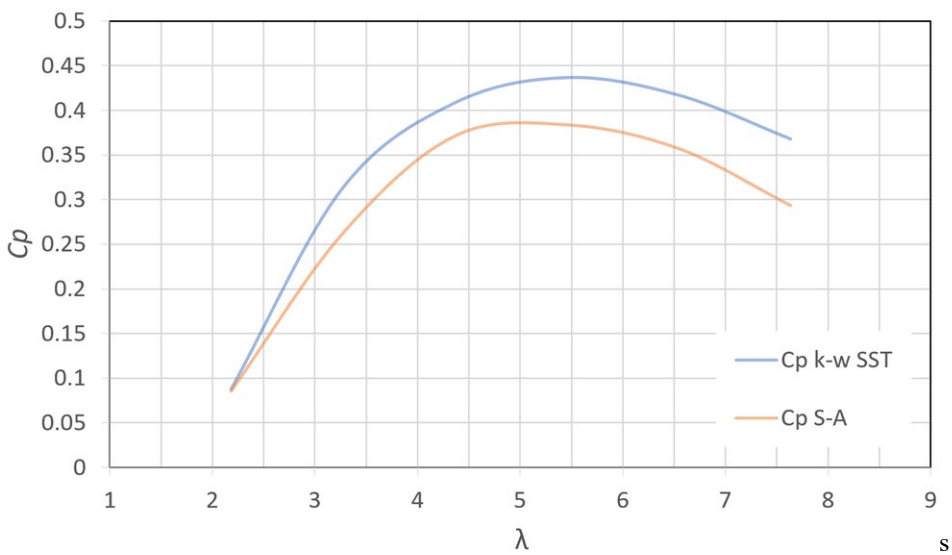

Figure 12: Results using the Sparlat Allmaras and K-omega SST models

For the purpose of verification, the results of this study and those of an experimental study by Monteiro et al. [35] for the same Piggot design in a wind tunnel are compared. In the experimental study, a peak Cp value of 0.388 was achieved (at a speed of 5.5 m/s) at a tip speed ratio (TSR) of 5.33. In this study, under the Sparlat Allmaras viscosity model, the maximum Cp value was recorded as 0.386 (at the same speed of 5.5 m/s) at a TSR of 5.10. This proved closer than the K-omega SST viscosity model, which returned a maximum Cp value of 0.437 (at the same speed of 5.5 m/s) at a TSR of 5.5. The Sparlat Allmaras viscosity model had an error value under 0.52%, which is acceptable for verifying the numerical analysis. In the research conducted by Monteiro et al., two computational simulations for the same design were carried out with WT_Perf and Qblade BEM codes. WT_Perf was developed by the US-based National Renewable Energy Laboratory (NREL) and is a software that is part of a suite of computer-aided engineering tools designed specifically for wind turbines. Qblade was first introduced in 2011 and has successfully been proven against WT_Perf and full-scale wind turbines' wind tunnel test data (Marten et al., 2013). As shown in Figure 13, the Qblade simulation recorded a maximum C_p value of 0.388 at a speed of 5.5 m/s. When the WT_Perf code was employed in the simulation, the C_p value rose to 0.394 [35].

Table 4: Summary of full model simulations and experimental results

Study	Value of C_p	Wind Speed (m/s)	Tip Speed Ratio	Error Percentage %
Experimental Study	0.388	5.5	5.33	-
Complete Model Study (with tower and hub) Sparlat Allmaras Viscosity Model	0.391	5.5	5.5	2.4
Complete Model Study (with tower and hub) K-omega SST Viscosity Model	0.44	5.5	5.5	15.2
Qblade Code Simulation	0.385	5.5	4.13	8
WT_Perf Code Simulation	0.396	5.5	4.45	4

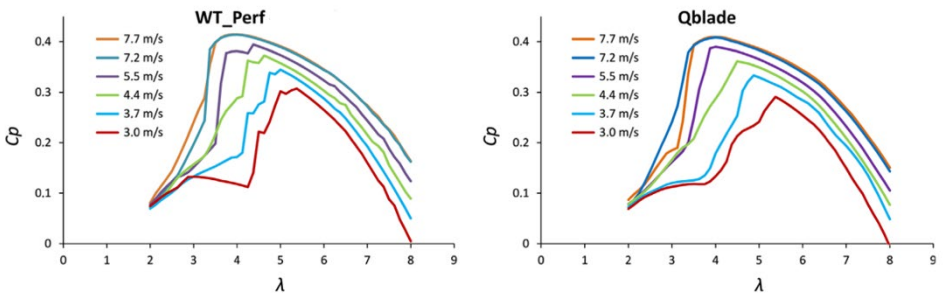

Figures 13: Results of the WT_Perf and Qblade codes [35]

4.2. Turbine Model Excluding Tower and Hub

This section attempts to simplify the geometry, decrease the computational domain, and reduce the time input. However, a focus is on safeguarding the accuracy of the results by ensuring they remain unaffected (or within an acceptable range).

In order to streamline the model, periodicity was utilized for a single blade in a 120-degree range. As illustrated in Figure 14, the simulation was conducted excluding a tower or hub. Figure 15 and Figure 16 show the Velocity and pressure results for partial model respectively.

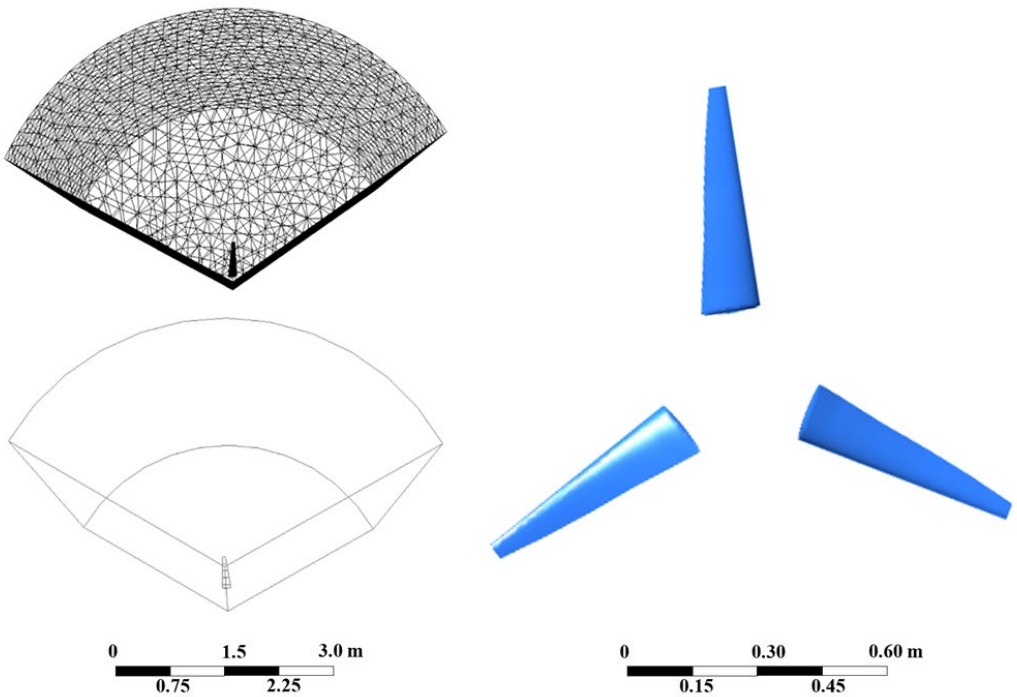

Figure 14: Turbine without the hub and tower

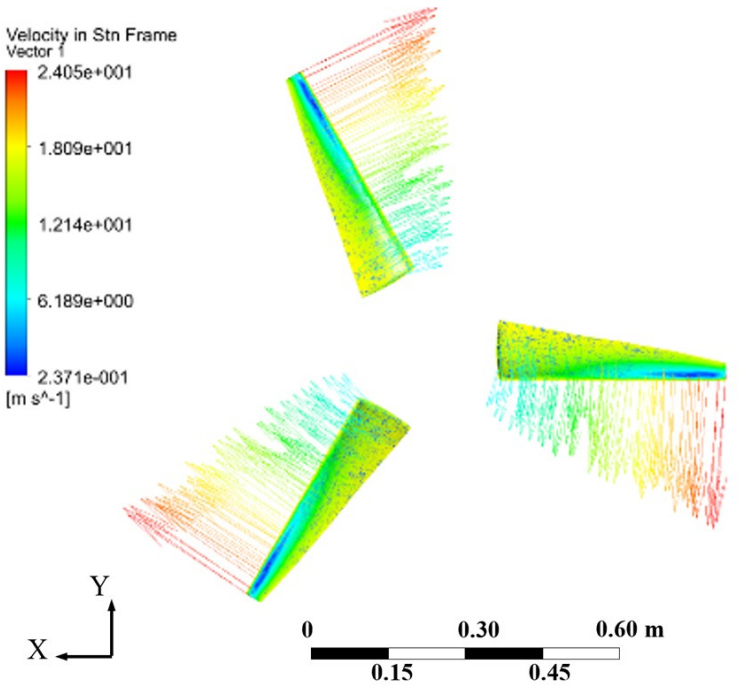

Figure 15: Velocity results for partial model

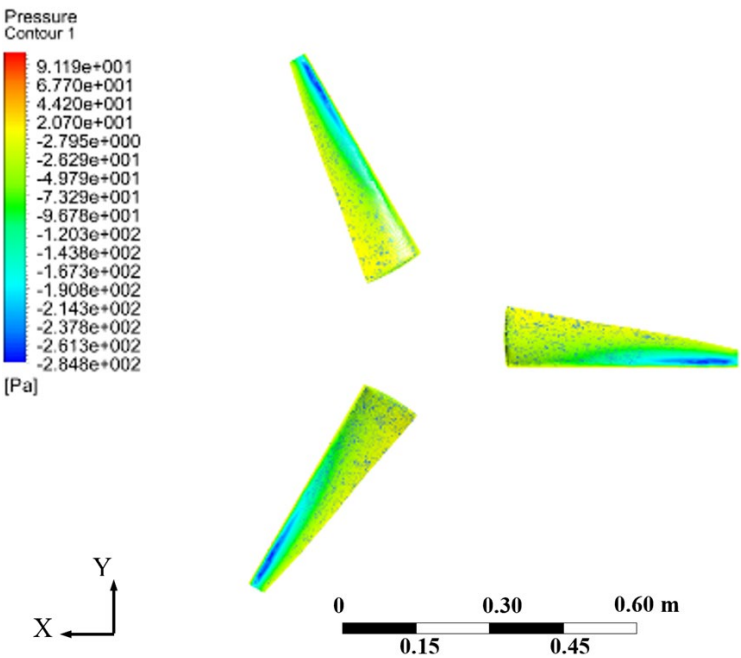

Figure 16: Pressure results for the partial model

The Sparlat Allmaras and K-omega SST viscosity models were employed for the full model simulations. The reason for this is that they have often been used in wind turbine simulations. For the partial model simulation, the Sparlat Allmaras viscosity model was selected as it was shown to generate results closer to the experimental results than were produced by the K-omega SST viscosity model. As certain components were excluded (i.e., the tower and hub) from the full model to form the partial model, it was necessary to develop a deeper study for the model to ensure its functionality as a turbine. Therefore, the power and torque coefficients were investigated and compared for the partial model utilising the following five input wind speeds: (i) 3 m/s; (ii) 3.7 m/s; (iii) 4.4 m/s; (iv) 5.5 m/s; (v) 7.2 m/s. These speeds correspond to the wind tunnel velocity values used in the experimental study. The K-epsilon viscosity model was eliminated as the results near the wall (i.e., the turbine) were inaccurate. The outlet is the pressure outlet, and Frame motion was utilized with the cell zone. In order to acquire the complete C_p vs. Tip Speed Ratio curve and C_q vs. Tip Speed Ratio curve, various rotational speeds were utilized. Figures 17 and 18 present all of the speed simulation results in graph format.

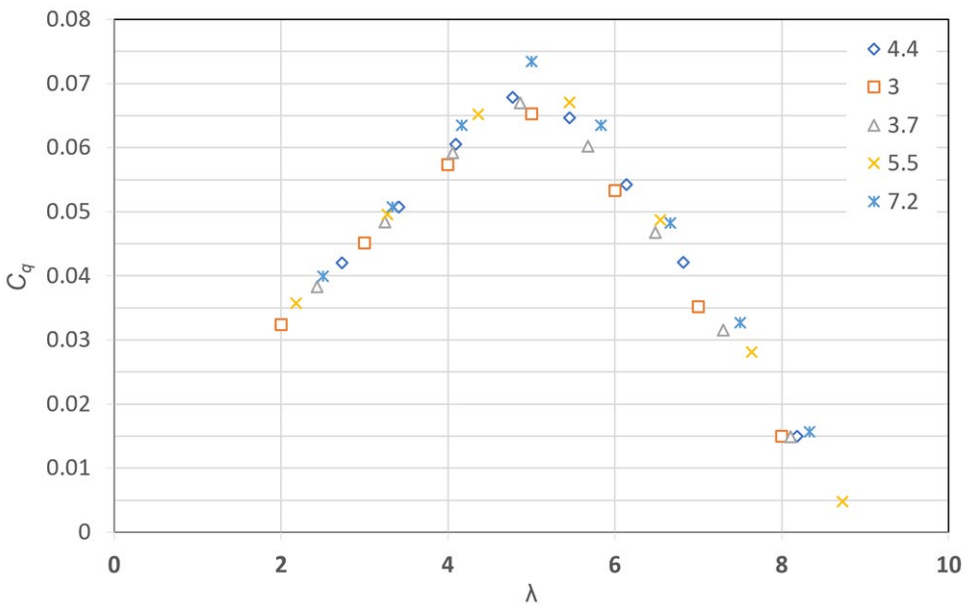

Figure 17: C_q vs. Tip Speed Ratio results for the turbine excluding the hub and tower

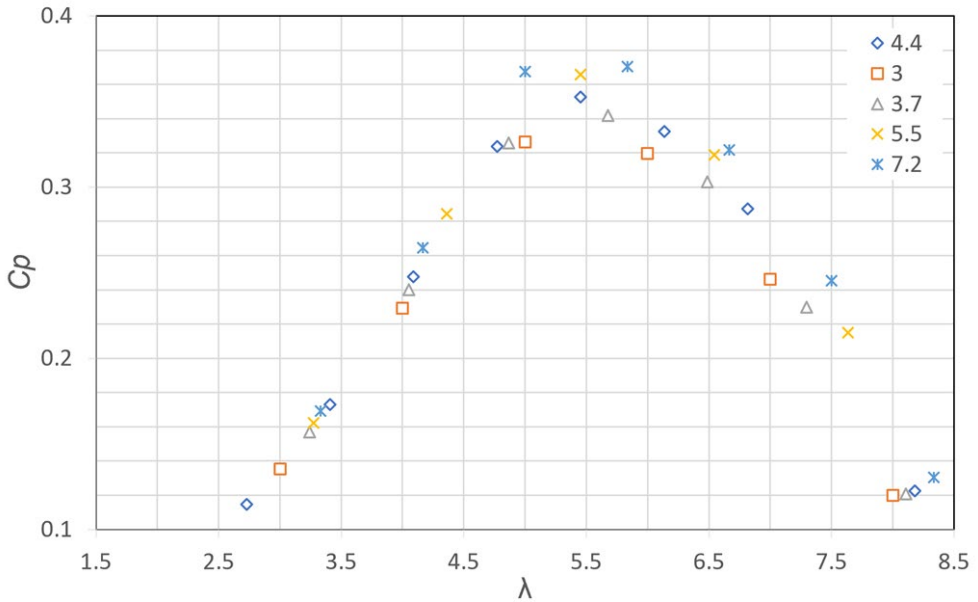

Figure 18: $\boldsymbol{Cp}$ vs. Tip Speed Ratio results for the turbine excluding the hub and tower

The results demonstrate reasonable values in comparison to the initial results of the complete model (which included hub and tower) in the wind tunnel. The curve acts as a normal Cp curve in which the power rises in line with the rotational speed. This means that the blade is functioning as a turbine. After a TSR of 5.83, the blade begins to function as a compressor, meaning that the flow over the blade starts to separate, thereby reducing the lift value. An important point here is that the wind turbine design is an upwind turbine, hence the presence of the tower and hub does not have a significant impact on the power or torque coefficients of the blade but does influence the wake analysis. These results compare directly with the experimental results [35]. In both this study and the experimental results, the maximum Cp values are 0.366 and 0.388, respectively, which equates to an error rate of 5.7%. Moreover, this study and the experimental study returned maximum C_q values of 0.068 and 0.072, respectively, equating to an error rate of 6%. This error was as expected due to the multitude of uncertainties and various strategies employed for the meshing and analysis. However, the approach and techniques used in this study are adequate for progressing to further analysis, as the error falls within an acceptable range. Employing more refined mesh and other convergence models will facilitate the minimization of the error rate. The simulation results are relatively comparable with those of other simulations [35] performed using two BEM codes. Figure 19 presents the results of a turbine that includes and excludes a hub.

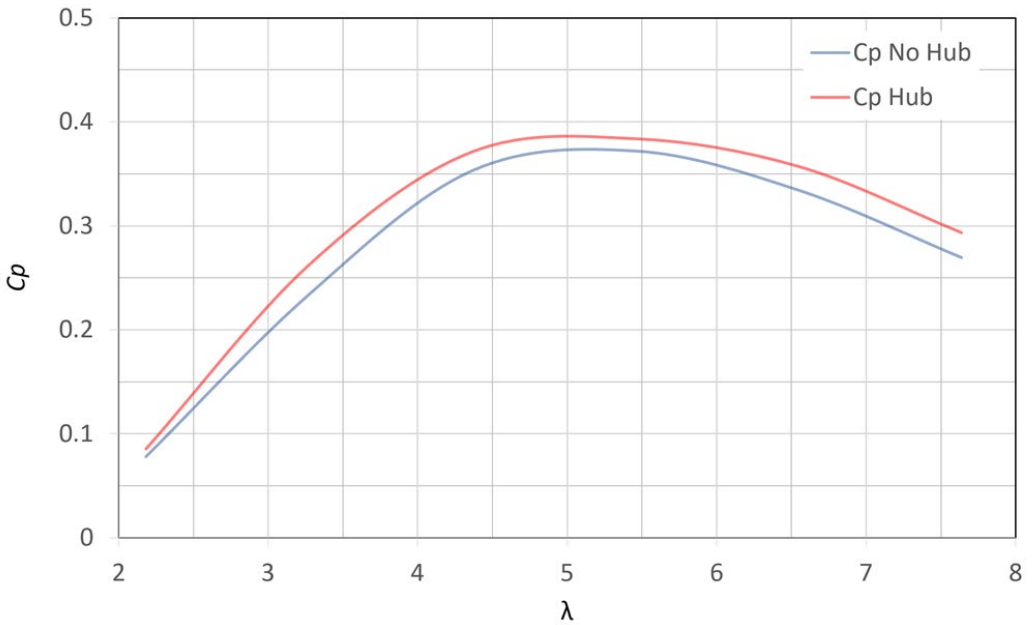

Figure 19: $\boldsymbol{Cp}$ vs. Tip Speed Ratio for speed 5.5 m/s (numerical)

The results of both the full and partial models are relatively similar to one another, meaning that the simplified model can be employed to calculate the turbines C_p graph. The underlying reason for this is that the hubs' rotational speed is very low due to the small radius. Consequently, the majority of the power is generated by the tip of the blade, while the hub part contributes little to the power torque. A difference of 5.2% for the C_p peak and 4.45% for the C_p value at a constant TSR of 5.5 were established in the results of the full and partial models. This is because the blade tip makes a much more significant contribution to the torque generation than the hub. When the hub is excluded, the air in the hub area does not impact the blade. Conversely, when the hub is included, the air moving towards the blade has been deflected by the hub, so consequently, there is greater airflow in the blade area close to the hub.

As illustrated above in Figure 20, both curves are fairly near to the experimental values [35], thereby validating the geometry and simulation construction. However, at higher TSR values, the experimental results tend to reduce much more rapidly, signifying that separation is much higher in reality. The reason for this is the physical models' rough surface. Table 5 shows a comparison of the results of the simulations and the experimental study at a precise TSR of 5.5 and wind speed of 5.5 m/s. Table 6 presents the comparisons with a maximum C_p value at the same 5.5 m/s wind speed.

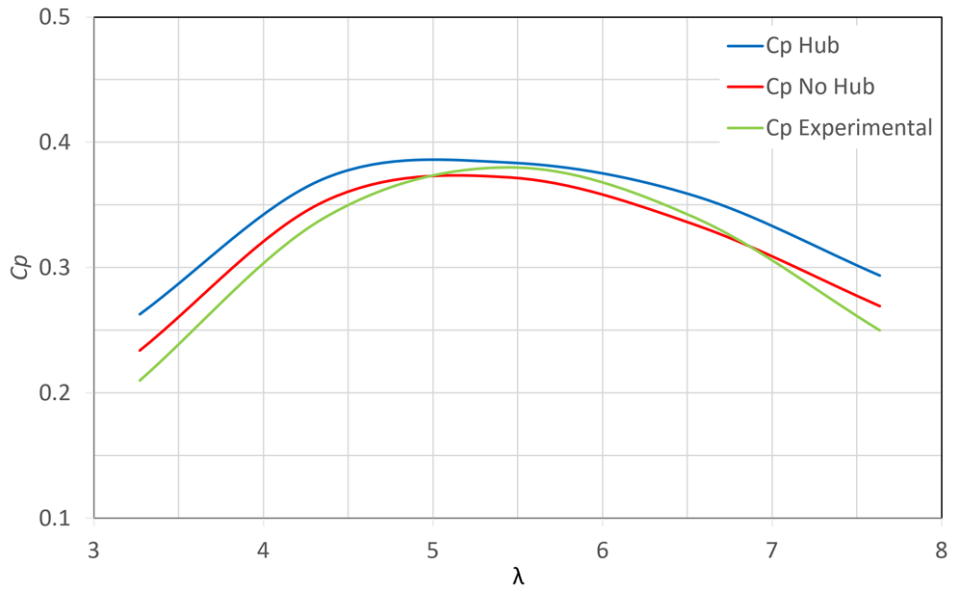

Figure 20: Total results compared with the experimental results

Table 5: Results summary (Cp values at a tip speed ratio of 5.5)

Study	**Value of C_p**	**Wind Speed (m/s)**	**Tip Speed Ratio**	**Error Percentage %**
Experimental Study	0.382	5.5	5.5	-
Complete Model Study (with tower and hub) Sparlat Allmaras Viscosity Model	0.383	5.5	5.5	0.3
Complete Model Study (with tower and hub) K-omega SST Viscosity Model	0.437	5.5	5.5	14.4
Simplified Model Study (without tower and hub)	0.366	5.5	5.5	4.2
Qblade Code Simulation	0.344	5.5	5.5	10
WT_Perf Code Simulation	0.35	5.5	5.5	8.4

Table 6: Results summary (Cp Peak)

Study	Value of C_p	Wind Speed (m/s)	Tip Speed Ratio	Error Percentage %
Experimental Study	0.388	5.5	5.33	-
Complete Model Study (with tower and hub) Sparlat Allmaras Viscosity Model	0.386	5.5	5.10	0.52
Complete Model Study (with tower and hub) K-omega SST Viscosity Model	0.437	5.5	5.50	12.6
Simplified Model Study (without tower and hub)	0.366	5.5	5.62	5.7
Qblade Code Simulation	0.388	5.5	4.00	0.0
WT_Perf Code Simulation	0.394	5.5	4.38	1.5

5. CONCLUSION

This study performed a numerical simulation for a complete horizontal axis wind turbine. It additionally analyzed a simplified model of the same turbine. Only a single blade was examined with rotational periodicity in the simplified model. In both cases, the results were established and verified with the available results of previous studies. In the complete model, the value was reported to be 0.386, while it was 0.366 in the simplified model. The error rate in the complete and simplified models was recorded at 0.52% and 5.7%, respectively. The study also achieved a 34% reduction in computational time.

Based on the results and findings of this study, it can be concluded that the simplified wind turbine model can facilitate the carrying out of any CFD analysis effectively, with accurate and reliable results. It can simultaneously significantly decrease the computational costs, especially in relation to wind farm simulation.

REFERENCES

[1] Wu Y-T, Liao T-L, Chen C-K, Lin C-Y, Chen P-W, Power output efficiency in large wind farms with different hub heights and configurations, Renewable Energy, March 2019, Vol. 132, pp. 941- 949.

[2] Gkeka-Serpetsidaki P, Tsoutsos T. A methodological framework for optimal siting of offshore wind farms: A case study on the island of Crete. Energy. Janary 2022, Vol. 239, Part D, 122296. DOI: https://doi.org/10.1016/j.energy.2021.122296

[3] Molina Gómez A, Morozovska K, Laneryd T, Hilber P, Optimal sizing of the wind farm and wind farm transformer using MILP and dynamic transformer rating, International Journal of Electrical Power and Energy Systems, March 2022, Vol. 136, 107645.

[4] Rak B. P., Santos Pereira R. B., Impact of the wake deficit model on wind farm yield: A study of yaw-based control optimization, Journal of Wind Engineering and Industrial Aerodynamics, Janary 2022, Vol. 220, 104827.

[5] Wu C., Luo K., Wang Q., Fan J., A refined wind farm parameterization for the weather research and forecasting model. Applied Energy, Janary 2022, Vol. 306, 118082.

[6] Schubel P. J., Crossley R. J., Wind Turbine Blade Design, Energies. September 2012, Vol. 5 (9), pp. 3425–3449.

[7] Archer C. L., Mirzaeisefat S., Lee S., Quantifying the sensitivity of wind farm performance to array layout options using large-eddy simulation, Geophysical Research Letters. September 2013, Vol. 40, pp. 4963 – 4970.

[8] Syed A. H., Javed A., Asim Feroz R. M., Calhoun R., Partial repowering analysis of a wind farm by turbine hub height variation to mitigate neighboring wind farm wake interference using mesoscale simulations, Applied Energy, June 2020, Vol. 268, 115050.

[9] Wang Q., Luo K., Yuan R., Zhang S., Fan J., Wake and performance interference between adjacent wind farms: Case study of Xinjiang in China by means of mesoscale simulations, Energy, January 2019, Vol. 166, pp.1168–1180.

[10] Yang X., Pakula M., Sotiropoulos F., Large-eddy simulation of a utility-scale wind farm in complex terrain, Applied Energy, November 2018, Vol. 229, pp. 767–777.

[11] Gasch R., Twele J., Wind Power Plants: Fundamentals, Design, Construction and Operation, Springer, Berlin, Heidelberg, 2012, Second Edition.

[12] Santos M., González M., Factors that influence the performance of wind farms, Renewable Energy, May 2019, Vol.135, pp. 643–651,

[13] Ragheb M., Ragheb A. M., Wind Turbines Theory - The Betz Equation and Optimal Rotor Tip Speed Ratio, Fundamental and Advanced Topics in Wind Power, July 2011, Chapter 2, pp.19-38.

[14] Gorban' A. N., Gorlov A. M., Silantyev V. M., Limits of the Turbine Efficiency for Free Fluid Flow, Journal of Energy Resources Technology, ASME, Decmber 2001, Vol. 123(4), pp. 311-317.

[15] Kalmikov A., Wind Power Fundamentals, Wind Energy Engineering: a Handbook for Onshore and Offshore Wind Turbines, Elsevier; 2017, pp. 17-24.

[16] Chehouri A., Younes R., Ilinca A., Perron J., Review of performance optimization techniques applied to wind turbines, Applied Energy, March 2015, Vol. 142, pp. 361-388.

[17] Antonini E. G. A., Romero D. A., Amon C. H., Improving CFD wind farm simulations incorporating wind direction uncertainty, Renewable Energy, April 2019, Vol. 133, pp.1011–1023.

[18] Naderi S., Parvanehmasiha S., Torabi F., Modeling of horizontal axis wind turbine wakes in Horns Rev offshore wind farm using an improved actuator disc model coupled with computational fluid dynamic, Energy Conversion and Management, September 2018, Vol. 171, pp. 953–968.

[19] Mahmuddin F., Rotor Blade Performance Analysis with Blade Element Momentum Theory, Energy Procedia, May 2017, Vol. 105, pp. 1123–1129.DOI: https://doi.org/10.1016/j.egypro.2017.03.477

[20] Nejadkhaki H. K., Sohrabi A., Purandare T. P., Battaglia F., Hall J. F., A variable twist blade for horizontal axis wind turbines: Modeling and analysis, Energy Conversion and Management, November 2021, Vol. 248,114771. DOI: https://doi.org/10.1016/j.enconman.2021.114771

[21] Abdelsalam A. M., El-Askary W. A., Kotb M. A., Sakr I. M., Experimental study on small scale horizontal axis wind turbine of analytically-optimized blade with linearized chord twist angle profile, Energy, February 2021, Vol. 216, 119304. DOI: https://doi.org/10.1016/j.energy.2020.119304

[22] Thangavelu S. K., Chow S. F., Sia C. C. V., Chong K. H., Aeroelastic performance analysis of horizontal axis wind turbine (HAWT) swept blades. Materialstoday: Proceedings, Janary 2021, Vol. 47, pp. 4965–4972. DOI: https://doi.org/10.1016/j.matpr.2021.04.315

[23] Shyam A., Aryan A. S., Shailesh C., Harigovind R., Vipin V., and Krishnan A., Design and analysis of small-scale horizontal axis wind turbine using PVC material, Materialstoday Proceedings, Vol. 52, Part 4, 2022, pp. 2238-2254. DOI: https://doi.org/10.1016/j.matpr.2021.08.095

[24] Wei D., Zhao W., Wan D., Xiao Q., A new method for simulating multiple wind turbine wakes under yawed conditions, Ocean Engineering, November 2021, Vol. 239, 109832. DOI: https://doi.org/10.1016/j.oceaneng.2021.109832

[25] Gao X., Li B., Wang T., Sun H., Yang H., Li Y., Wang Y., Zhao F., Investigation and validation of 3D wake model for horizontal-axis wind turbines based on filed measurements, Applied Energy, Feburary 2020, Vol. 260, 114272. DOI: https://doi.org/10.1016/j.apenergy.2019.114272

[26] Prabowoputra D. M., Prabowo A. R., Bahatmaka A., Hadi S., Analytical Review of Material Criteria as Supporting Factors in Horizontal Axis Wind Turbines: Effect to Structural Responses, Procedia Structural Integrity, Janary 2020, Vol. 27, pp. 155 - 162. DOI: https://doi.org/10.1016/j.prostr.2020.07.021

[27] Qi Y., Xu S., Huang D., Investigation on aerodynamic performance of horizontal axis wind turbine by setting micro-plate in front of the blade leading edge, Renewable Energy, December 2021, Vol. 179, pp. 2309–2321. DOI: https://doi.org/10.1016/j.renene.2021.08.035

[28] Regodeseves P. G., Morros C. S., Numerical study on the aerodynamics of an experimental wind turbine: Influence of nacelle and tower on the blades and near-wake, Energy Conversion and Management, June 2021, Vol. 237, 114110. DOI: https://doi.org/10.1016/j.enconman.2021.114110

[29] Guo T., Guo X., Gao Z., Li S., Zheng X., Gao X., Rennian L., Wang T., Li Y., Li D., Nacelle and tower effect on a stand-alone wind turbine energy output—A discussion on field measurements of a small wind turbine, Applied Energy, December 2021, Vol. 303, 117590. DOI: https://doi.org/10.1016/j.apenergy.2021.117590

[30] Gao Z., Li Y., Wang T., Shen W., Zheng X., Pröbsting S., Li D., Li R., Modelling the nacelle wake of a horizontal-axis wind turbine under different yaw conditions, Renewable Energy. July 2021, Vol. 172, pp. 263–275. DOI: https://doi.org/10.1016/j.renene.2021.02.140

[31] Abraham A., Dasari T., Hong J., Effect of turbine nacelle and tower on the near wake of a utility-scale wind turbine, Journal of Wind Engineering and Industrial Aerodynamics, October 2019, Vol. 193, 103981. DOI: https://doi.org/10.1016/j.jweia.2019.103981

[32] Zhu X., Sun C., Ouyang H., Du Z., Numerical investigation of the effect of towers and nacelles on the near wake of a horizontal-axis wind turbine model, Energy, Janary 2022, Vol. 238, 121782. DOI: https://doi.org/10.1016/j.energy.2021.121782

[33] Caldichoury, M. Souli, E. Sarradj, T. Geyer, F. Del Pin, Numerical investigation of flow around hairy flaps cylinder using FSI Capabilities, International journal of Multiphysics, 2018, Vol. 12, No. 2, DOI: https://doi.org/10.21152/1750-9548.12.2.189

[34] Zienkiewicz O. C., Taylor R. L., Nithiarasu P., Turbulent Flows, The Finite Element Method for Fluid Dynamics, Chapter 8, 2014, 7th Edition, pp. 283–308. DOI: https://doi.org/10.1016/B978-1-85617-635-4.00008-X

[35] Monteiro J. P., Silvestre M. R., Piggott H., André J. C., Wind tunnel testing of a horizontal axis wind turbine rotor and comparison with simulations from two Blade Element Momentum codes, Journal of Wind Engineering and Industrial Aerodynamics, December 2013, Vol. 123, pp. 99–106. DOI: https://doi.org/10.1016/j.jweia.2013.09.008